RESEARCH ARTICLE

NANO · MICRO small
www.small-journal.com

Dynamic Structural Change of Plant Epidermal Cell Walls under Strain

Jingyi Yu, Joshua T. Del Mundo, Guillaume Freychet, Mikhail Zhernenkov, Eric Schaible, Esther W. Gomez,* Enrique D. Gomez,* and Daniel J. Cosgrove*

The molecular foundations of epidermal cell wall mechanics are critical for understanding structure–function relationships of primary cell walls in plants and facilitating the design of bioinspired materials. To uncover the molecular mechanisms regulating the high extensibility and strength of the cell wall, the onion epidermal wall is stretched uniaxially to various strains and cell wall structures from mesoscale to atomic scale are characterized. Upon longitudinal stretching to high strain, epidermal walls contract in the transverse direction, resulting in a reduced area. Atomic force microscopy shows that cellulose microfibrils exhibit orientation-dependent rearrangements at high strains: longitudinal microfibrils are straightened out and become highly ordered, while transverse microfibrils curve and kink. Small-angle X-ray scattering detects a 7.4 nm spacing aligned along the stretch direction at high strain, which is attributed to distances between individual cellulose microfibrils. Furthermore, wide-angle X-ray scattering reveals a widening of (004) lattice spacing and contraction of (200) lattice spacing in longitudinally aligned cellulose microfibrils at high strain, which implies longitudinal stretching of the cellulose crystal. These findings provide molecular insights into the ability of the wall to bear additional load after yielding: the aggregation of longitudinal microfibrils impedes sliding and enables further stretching of the cellulose to bear increased loads.

1. Introduction

Plant cells grow by extending their primary cell walls under cell turgor and can achieve surface area expansions greater than 100-fold during their lifetime.[1] The mechanical properties of the primary cell wall therefore strongly affect plant growth and morphogenesis.[2] Epidermal cell walls, which limit the growth of plant cells and control the overall shape of the plant, are extensively used for primary cell wall research due to their simple geometry and ease of sample preparation. Studies of epidermal cell wall microstructure in tandem with mechanical studies can bridge the gap between the physical properties of cell walls and underlying polymer interactions. Additionally, elucidating the molecular mechanisms regulating the extensibility and strength of epidermal cell walls helps us to understand the mechanical properties of hierarchically structured cellulosic materials and paves the way for the design of bioinspired materials.

J. Yu, D. J. Cosgrove
Department of Biology
Pennsylvania State University
University Park, PA 16802, USA
E-mail: juy323@psu.edu
J. T. Del Mundo, E. W. Gomez, E. D. Gomez
Department of Chemical Engineering
Pennsylvania State University
University Park, PA 16802, USA
E-mail: ewg10@psu.edu; edg12@psu.edu
G. Freychet, M. Zhernenkov
National Synchrotron Light Source II
Brookhaven National Laboratory
Upton, NY 11973, USA
E. Schaible
Advanced Light Source
Lawrence Berkeley National Laboratory
1 Cyclotron Road, Berkeley, CA 94720, USA
E. W. Gomez
Department of Biomedical Engineering
Pennsylvania State University
University Park, PA 16802, USA
E. D. Gomez
Department of Materials Science and Engineering
Pennsylvania State University
University Park, PA 16802, USA
E. D. Gomez
Materials Research Institute
Pennsylvania State University
University Park, PA 16802, USA

The ORCID identification number(s) for the author(s) of this article can be found under https://doi.org/10.1002/smll.202311832

DOI: 10.1002/smll.202311832

The outer epidermal walls of onion scales can be isolated as a sheet of cell walls in a planar geometry, providing a platform to study cell wall structures and mechanics.[3,4] This system is structured in a cross-lamellate fashion with each lamella consisting of roughly aligned cellulose microfibrils (CMFs) bound with xyloglucan in a gel-like pectin matrix. The orientation of CMFs between adjacent lamellae is expected to change within the range of 30° to 90°,[5] which would result in an overall isotropic CMF alignment in the wall. However, it has been observed that tensile properties vary quantitatively along the longitudinal and transverse directions,[6,7] suggesting some degree of anisotropy. Onion epidermal cells typically have a large aspect ratio, with the long axis of the cell aligned with the top-to-bottom axis of the onion bulb. Here, we refer to the axis parallel to the long side of the cells as "longitudinal" and the perpendicular axis as "transverse." Furthermore, we expect there to be a detectable change in anisotropy from its initial state after extension.

The organization of and interactions between cell wall components determine the mechanical properties of the cell wall. CMFs are thin (≈3 nm wide), rigid, semicrystalline rods thought to be the major load-bearing component in the primary cell wall. A recent coarse-grained model of onion epidermal wall revealed that load-bearing mechanics are predominately governed by cellulose-cellulose contacts between microfibrils, with pectin and xyloglucan making little direct contribution to tensile mechanics.[8] Simulation of microfibril movements during stretching showed that these movements depend on the initial microfibril orientation relative to the stretch direction. Microfibrils that were initially oriented roughly parallel to the stretch axis straightened, reoriented and slipped, while those that were roughly perpendicular to the stretch axis curved. It was found that cellulose-cellulose sliding motions contributed the most to plastic deformation. However, the coarse-grained model only explored strains up to 12%, slightly beyond the yield point. The molecular rearrangements of wall polymers after extensive irreversible wall extension need further investigation.

The mechanical properties of onion epidermal walls are complex. Under tensile strain, the wall undergoes elastic stiffening and starts to yield as the stress reaches a threshold. As yielding continues, the wall requires even more stress for further plastic deformation.[9] This contradicts the expectation that as fibers begin to slide, their contact area should decrease, requiring less stress for additional sliding. The molecular mechanism of this behavior in cellulose materials remains uncertain. Previous wall modeling studies show that CMFs are drawn together upon tensile stretching,[8] which may result in the formation of larger CMF bundles that are less prone to slippage and capable of bearing higher loads. However, there is no experimental evidence showing that CMFs form larger bundles upon extensive deformation (>20% strain).

Atomic force microscopy (AFM) can resolve CMF bundles and has been extensively utilized to image the innermost lamella in onion epidermal peel. In situ AFM of cell walls undergoing extension demonstrated a variety of CMF movements, including reorientation, sliding, and kinking.[10] While AFM is invaluable for its ability to map surface CMF features, it is difficult to probe lamellae below the surface. Therefore, we propose that bulk transmission measurements should complement AFM to examine CMF organization throughout the cell wall. Previous studies have shown the effectiveness of bulk measurements such as X-ray scattering and transmission-polarized Fourier transform infrared spectroscopy in characterizing the re-orientation of cellulose and pectin upon stretch or during development.[7,11,12]

Small-angle X-ray scattering (SAXS) and wide-angle X-ray scattering (WAXS) are nondestructive, fast acquisition bulk characterization techniques, which together provide a plethora of structural information over a wide range of length scales. SAXS can probe ordered microfibril packing and bundling due to the density contrast between cellulose and pectin. In conjunction, WAXS can probe cellulose unit cell parameters, which relate to the packing of cellulose chains within the crystal. The use of an area detector can also map the CMF angle distribution, which is invaluable for mechanical studies.[13,14] These techniques have commonly been used in situ with tensile testing to probe structural dynamics in polymeric materials, including those derived from cellulose.[15]

Despite the value of in situ SAXS/WAXS measurements, the low sample scattering and high background from humid air can make these experiments difficult. Instead, we developed a method to preserve the structures of fibrils prior to data acquisition. Upon dehydration, the wall experiences negligible changes in length (<1%) and width (<2%) as well as negligible changes in the nanostructure.[16,17] Therefore, we preserve the face-view alignment of CMFs as the matrix becomes hard and rigid upon dehydration.[16] Dried samples are more easily incorporated into a minimal background scattering sample environment, typically vacuum or helium.

Seeking to understand the reorganization of cell wall polymers from the mesoscale to molecular scale during cell wall extension, we characterized structures of walls stretched to different strain levels using optical microscopy, AFM, SAXS, and WAXS. Our results show that upon extensive deformation, CMFs realign and pack more tightly, which allows cellulose crystals to undergo additional stretching and bear more load even after the wall starts to yield. These findings shed light on the structural dynamics of wall polymers and the molecular mechanisms of the ability of cell walls to deform extensively without compromising their load-bearing capacity.

2. Results

2.1. Dimensional Change of Cell Wall upon Deformation

To study the structural change of wall polymers under different degrees of deformation, we stretched the isolated onion epidermal walls (≈7 µm thick) uniaxially along the long axis of onion cell profiles (**Figure 1A**) to target strains ranging from 5% to 45% (Figure 1B). The wall shows nonlinear stress responses upon deformation (1st pulls), indicative of dynamic structural rearrangement of wall polymers. Upon initial stretching (<5%), the wall modulus (the slope of the stress-strain curve), indicative of the wall stiffness, increases, and the deformation is elastic. Beyond 5%, the wall starts to yield but still requires higher stresses to be further stretched, a phenomenon known as "strain hardening." As the strain increases beyond ≈20%, the wall exhibits a linear stress–strain curve with increasing stress ("linear plastic deformation"). To examine this behavior and the organization of cellulose at multiple size scales at large strains, we characterized

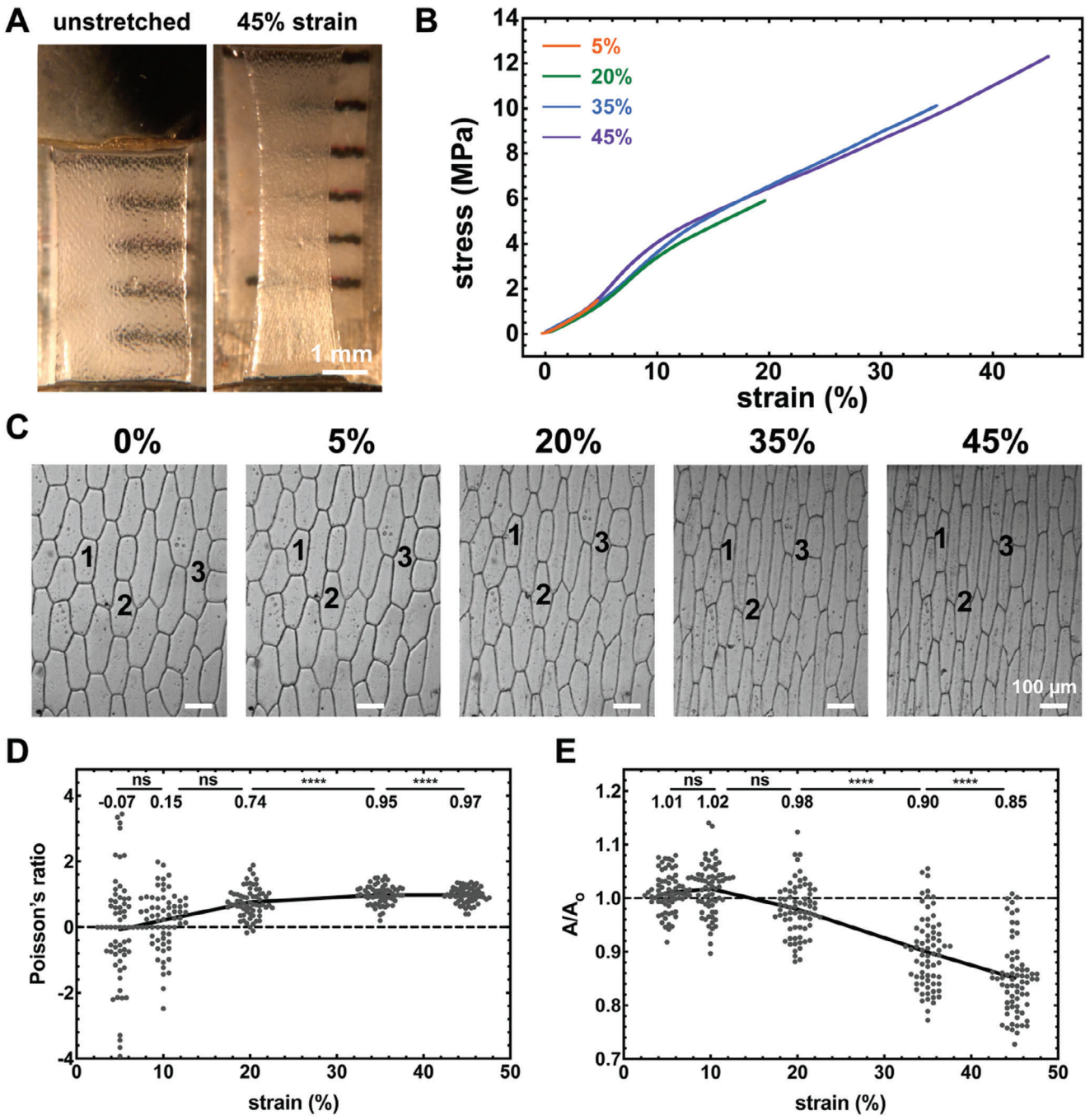

Figure 1. Deformation of epidermal cell walls upon strain. A) Onion peel samples mounted on the stretching device in an unstretched state and at a strain of 45%. B) Stress–strain curves of the walls stretched to different target strains. Loadings to different target strains were from different wall samples of the same onion. C) Microscopy images showing cell deformation of epidermal walls stretched to different strains. 1, 2, and 3 indicate specific cells. D) Poisson's ratio of walls stretched to 5%, 10%, 20%, 35% and 45% ($n = 65$ cells). E) Normalized cell wall area for walls stretched to 5%, 10%, 20%, 35% and 45% ($n = 70$). Each dot represents a measurement from one cell. T-tests were conducted between measurements from consecutive strains. "ns" means no significant difference while "****" indicates a significant difference with a p-value < 0.0001.

the structure of walls stretched to strains ranging from 5% to 45%.

Upon uniaxial stretching, the wall extends along the stretching direction but shrinks in the transverse direction (Figure 1A). To further quantify the dimensional change of the wall shape, we stretched the wall under the microscope and visualized the wall deformation at the microscale. The wall deforms as an intact material without cell separation or slippage (Figure 1C). Each cell extends in the longitudinal direction while contracting in the transverse direction as the strain increases. The change in cell

shape was quantified with the in-plane Poisson's ratio (the negative transverse strain divided by the longitudinal strain). We measured the longitudinal and transverse strain at the single-cell level and plotted the Poisson's ratio as a function of strain (Figure 1D). The in-plane Poisson's ratio is below 0.2 at small strains and increases close to 1 as the strain approaches 35%, showing that the transverse contraction of the wall is more prominent at large strains. To examine the effects of reshaping on the wall area, we measured the epidermal wall area of each cell (delineated by the anticlinal wall) at different strains (Figure 1E). The wall area stays constant at small strains but starts decreasing from 20% strain. Decreased wall area suggests an increase in wall polymer density, where polymers may come into closer proximity and form new contacts as water moves out and the wall matrix is compressed. Overall, dimensional analysis shows that from 20% strain and beyond, the wall reshapes and contracts in the width direction to the extent that the wall area starts to decrease. This implies that the CMF networks may undergo large-scale rearrangement to facilitate the reshaping of the entire cell wall upon tensile stretching.

2.2. AFM Revealed the Rearrangement of CMF Networks

To characterize the wall polymer rearrangement upon large deformation, we stretched the wall to target strains ranging from 5% to 50% and fixed the polymer structures by air-drying the walls, which were then further examined with AFM and X-ray scattering. The walls stretched and dried under tension at the target strains show overall rearranged wall structures (**Figure** 2A), whereas the walls that were stretched and relaxed before drying only contain the plastic structural changes (Figure 2B).

To examine the rearrangement of CMF networks upon deformation, we used AFM to visualize the surface cellulose microfibril features. This was achievable by lightly digesting the samples with pectate lyase to remove the surface pectin layer.[5] AFM height images of unstretched walls show CMF bundles oriented in preferential directions in different lamellae (**Figure** 3A,F), similar to the multi-lamellate cellulose network observed in hydrated walls.[18] In the walls stretched to 5%, no significant change in the CMF arrangements is observed (Figure 3B,G). As the walls were stretched to 20% and beyond, CMFs started to show two major orientation-dependent features. In some cases, the surface CMFs align towards the longitudinal direction (stretching direction), adopting straightened and stretched-out configurations (see CMFs marked in blue in Figure 3C–E), enabling them to bear forces in the stretching direction. In other cases, the surface CMFs are transversely oriented (perpendicular to the stretching direction) and exhibit curved or kinked appearances (see CMFs marked in green in Figure 3H–J). These CMFs do not provide resistance to the longitudinally applied stress and likely undergo curving to accommodate the overall change in wall shape. In some cases, we observed transversely curved CMFs in the top lamella and longitudinally stretched CMFs in the underneath lamella (Figure 3I). This shows that as the wall is stretched beyond 20% and deforms, CMFs exhibit two distinct patterns of rearrangement based on their orientation relative to the stretching direction.

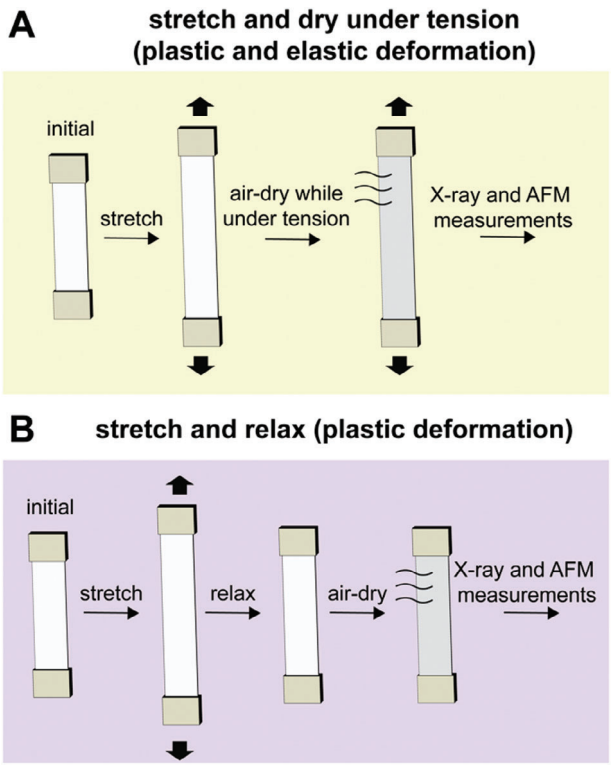

Figure 2. Schematic of mechanical treatment processes for onion outer epidermal peel samples. A) For observation of both elastic and plastic polymer deformation, the walls were stretched and fixed by air-drying under tension. B) For observation of plastic polymer deformations, the walls were stretched and relaxed from tension before air drying.

To further analyze the degree of alignment of longitudinally oriented CMFs at large strains, we measured the orientation distribution of CMFs from the AFM images. As the target strain increases, CMFs align more uniformly (Figure 3K). As CMFs move closer together during realignment, they do not aggregate into macrobundles,[19,20] but remain as thin bundles or individual CMFs that are distinctively visible and well resolved (Figure 3C–E). Overall, in contrast to the slightly wavy and separated CMF networks observed in the unstretched and 5% strained walls, large deformations cause the CMFs along the stretching direction to align more uniformly, resulting in the formation of a well-ordered cellulose network.

The reversibility of these CMF features was examined by imaging walls that were stretched to 50%, released, and allowed to relax prior to drying, such that only irreversible perturbations to the CMF structure would be apparent (Figure 3N); about 20% residual deformation was present prior to drying. In the stretched-then-relaxed walls, some transversely aligned CMFs still appear kinked and curved in a few locations and the CMFs become more disorganized overall. On the other hand, the highly ordered CMF network in the walls stretched beyond 20% is absent. As shown in the distribution plot (Figure 3K), CMFs in stretched-relaxed walls appear less aligned compared with those in highly strained walls. This indicates that the kinking of transverse CMFs may be partially irreversible, while the ordered alignment of longitudinal CMFs is reversed upon removal of the load.

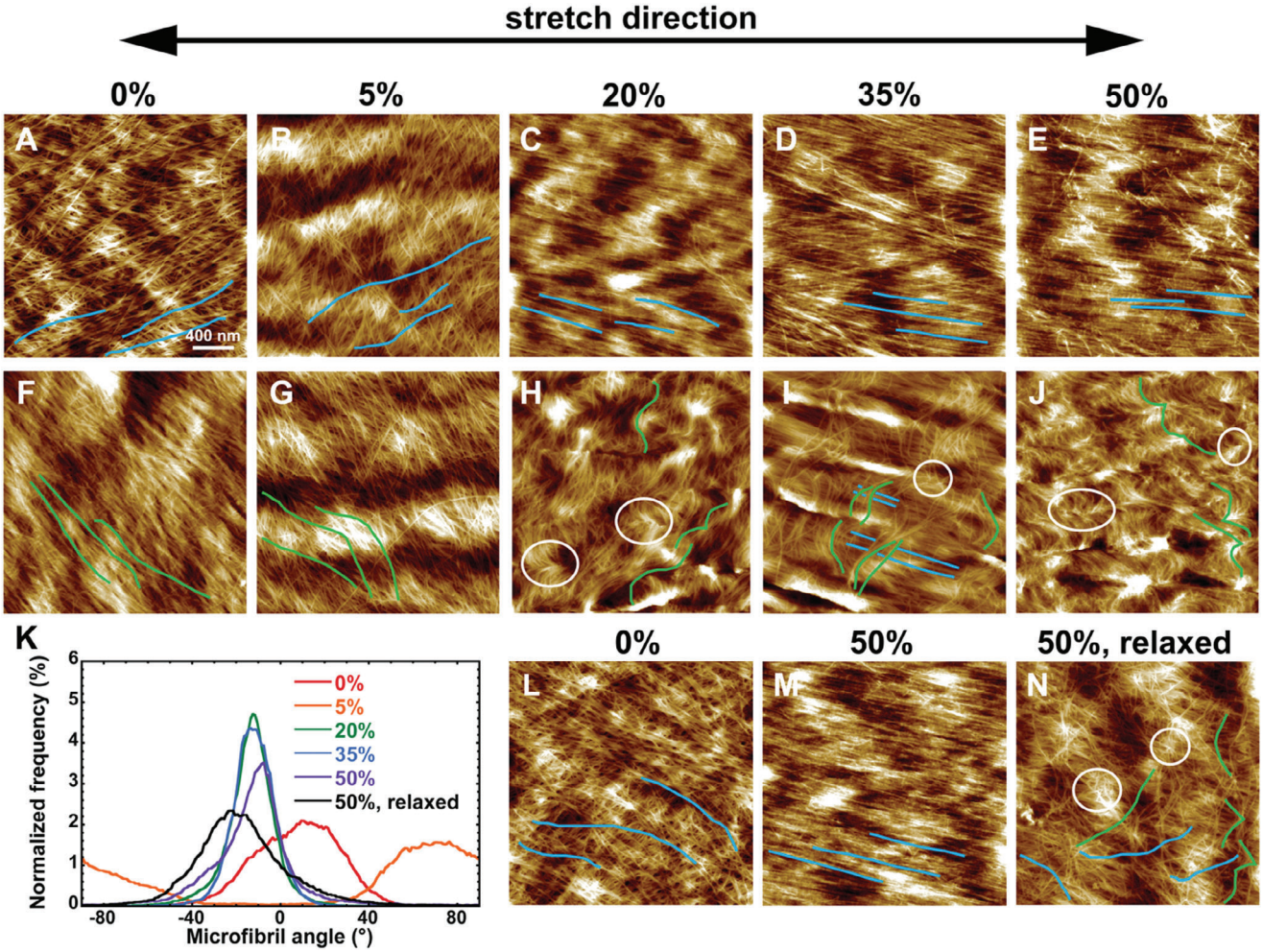

Figure 3. AFM images of onion epidermal walls stretched and dried at various strains show differential surface CMF features. A,F) unstretched and B,G) 5% stretched walls show relaxed and spaced-out CMF bundles in different lamellae. Upon large deformation, the wall shows two orientation-dependent features: CMFs preferentially oriented toward the stretching direction are straightened out and become highly aligned in the C) 20%, D) 35%, and E) 50% stretched walls, as shown in CMFs marked in blue; CMFs preferentially oriented perpendicular to the stretching direction appear curved (marked in green) or kinked (highlighted in white circle) in the H) 20%, I) 35% and J) 50% stretched walls. K) Orientation distribution of surface CMFs in walls stretched to different strains (correspond to images A–E and N). Surface CMF features of L) unstretched, M) 50% stretched and N) 50% stretched then relaxed walls reveal plastic changes in CMF organization. Blue marks some CMFs oriented longitudinally while green marks some CMFs oriented transversely.

2.3. CMF Realignment and Ordering (SAXS)

Analysis of transmission X-ray scattering complements the surface information from AFM by probing the ordered structures and fibril orientation throughout the entire thickness of the wall. SAXS intensities arise from spatial correlations between domains, where we expect that the contrast between crystalline microfibrils and less dense matrix polysaccharides (e.g., pectin) dominates. We probed length scales between about 0.3 to 60 nm at the Soft Matter Interfaces (SMI) beamline of the National Synchrotron Light Source II (NSLS-II) located in Brookhaven National Laboratory and at beamline 7.3.3 of the Advanced Light Source (ALS) located in Lawrence Berkeley National Laboratory.[21] Scattering intensities at scattering vector q ($q = 4\pi\sin(\theta)/\lambda$, where θ is half of the scattering angle and λ is the X-ray wavelength) correspond to microstructural features such as center-to-center distances between microfibrils. 2D SAXS images were acquired for peels that were stretched to a specified strain and dried under tension (**Figure** 4A–E, SMI, NSLS-II) and for onion peels that were stretched to 45% and then relaxed with residual strains of ≈15% (Figure 4F,G, 7.3.3, ALS). The unstretched peels (Figure 4A,F) show slightly higher scattering in the direction perpendicular to the long cell axis, suggesting a small net preference for fibrils to align with the long cell axis.

Figure 4H shows scattering intensity integrated at 0.01 $Å^{-1} < q < 0.1$ $Å^{-1}$ versus azimuthal angle for onion peels that were stretched and dried under tension (SMI, NSLS-II), where 0° corresponds to the horizontal (equatorial) direction in the 2D images. Intensity at 0° in the azimuthal intensity profiles corresponds to CMFs that are aligned with the long axis of the onion cell. The full width at half maximum (FWHM) around 0° quantitatively describes the degree of CMF alignment and is inversely

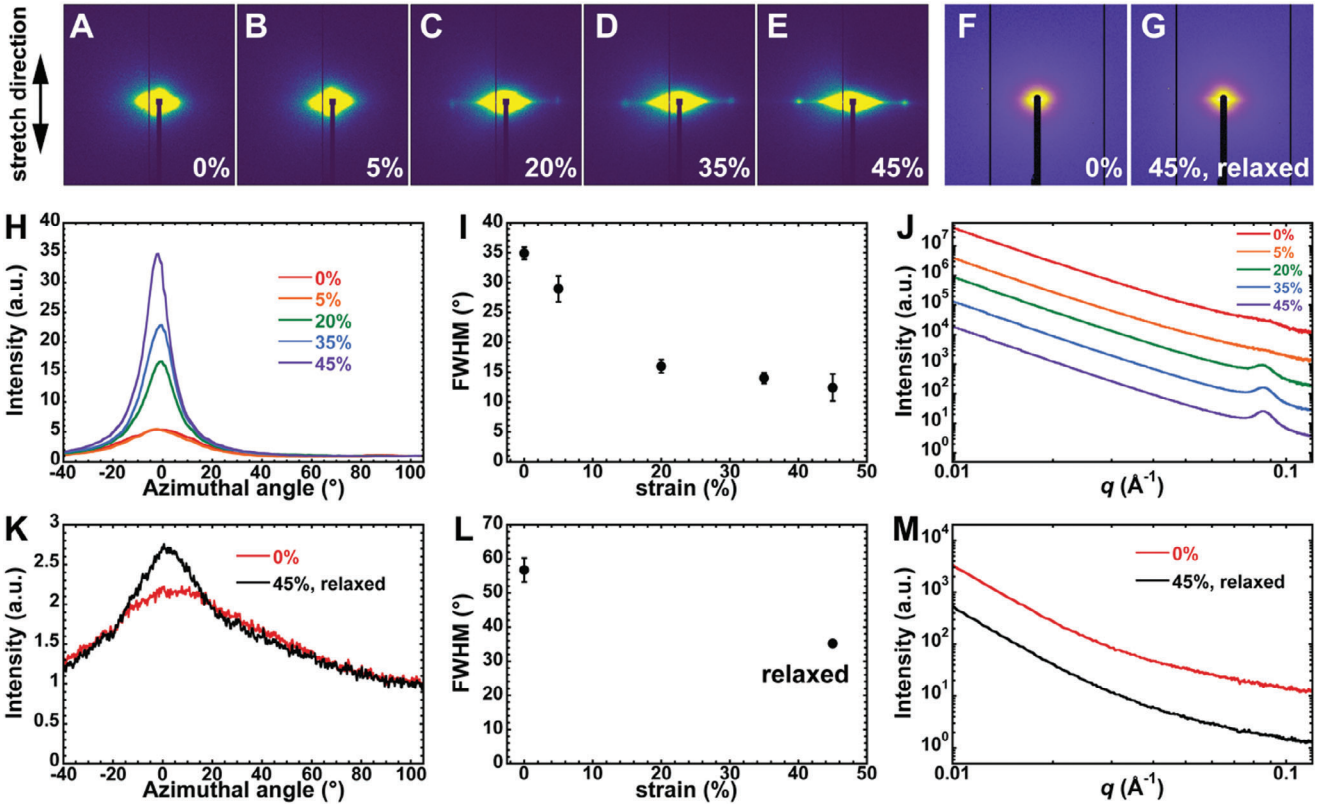

Figure 4. Transmission small-angle X-ray scattering reveals changes in the ordering and orientation of nanoscale structures. SAXS 2D images of A) unstretched, B) 5%, C) 20%, D) 35%, and E) 45% strain onion epidermal wall, taken at the Soft Matter Interfaces beamline at National Synchrotron Light Source II, Brookhaven National Laboratory. 2D SAXS images of F) unstretched and G) 45% strain then relaxed onion epidermal wall, taken at beamline 7.3.3 at Advanced Light Source, Lawrence Berkeley National Laboratory. H) Azimuthal intensity profiles, I) FWHM of azimuthal intensity profiles, and J) sector profiles of the unrelaxed samples. K) Azimuthal intensity profiles, L) FWHM of azimuthal intensity profiles, and M) sector profiles of the relaxed samples. Azimuthal intensity profiles integrated at $0.01\ \text{Å}^{-1} < q < 0.1\ \text{Å}^{-1}$. For comparison, H,K) azimuthal intensity profiles were normalized at 100°. Data points represent mean ± SEM for three replicates. Sector profiles are integrated at ± 5° along the equatorial direction. J,M) Sector profiles are offset for comparison. All curves represent an average of three replicates.

proportional to the degree of longitudinal CMF alignment. From 0 to 45% strain, the width of the azimuthal intensity profiles decreases from 34.9 ± 1.0° to 12.4 ± 2.3° (mean ± standard error of the mean) (Figure 4I), resulting in a 64% reduction in FWHM ($p < 0.01$, $n = 3$). The largest jump in FWHM observed was 11.5° between 5% and 20% strain ($p < 0.01$, n = 3). For comparison, the samples stretched and dried under tension were also measured at beamline 7.3.3 of ALS, which resulted in a change in FWHM from 39.2 ± 1.1° to 17.1 ± 1.5° for 0% and 45% respectively, a 56% decrease ($p < 0.01$, $n = 3$).

Once 20% strain was reached, a diffraction peak was observed in the equatorial direction, which is visible as spots in the equatorial regions of Figure 4C–E. SAXS equatorial profiles versus q (Figure 4J) show that the peak is at 0.085 Å^{-1}, corresponding to a 7.4 nm wide spacing parallel to the stretch direction ($d = 2\pi/q$). This finding is consistent with the AFM observations, where CMFs become more ordered in the stretching direction after large deformation but return to a more spaced-out and disordered arrangement after relaxation. A 7.4 nm spacing is consistent with individual cellulose microfibrils packed closely together, where the high degree of alignment in the microfibril axis leads to the strong scattering signal that is apparent in Figure 4J. The diffraction spot at 0.085 Å^{-1} in the SAXS data collected at the ALS was also observed for onions stretched at 45% strain (Figure S1, Supporting Information).

Figure 4K shows that upon relaxation from 45% strain, the scattering exhibits a slight increase in anisotropy (7.3.3, ALS). The FWHMs of the azimuthal intensity profiles were 56.8 ± 3.5° and 35.2 ± 0.1° for the 0% and 45% relaxed samples, respectively (Figure 4L), a 38% reduction in FWHM ($p < 0.05$, $n = 3$). This reduction in FWHM is notably less than those of peels that were stretched and dried under tension. The difference between the widths of the 0% strain control samples for the relaxed deformation and unrelaxed datasets (Figure 4A,F) may be due to biological variation among samples and/or to differences in background scattering and beam broadening, as the two experiments were conducted at different beamlines. Overall, we can conclude that samples that are not allowed to relax exhibit greater CMF reorientation than samples that relax, indicating that a considerable amount of CMF reorientation remains reversible at high strain. The equatorial sector profiles of the relaxed samples (Figure 4M) appeared to be featureless, indicating that the 7.4 nm spacing feature is also a reversible rearrangement.

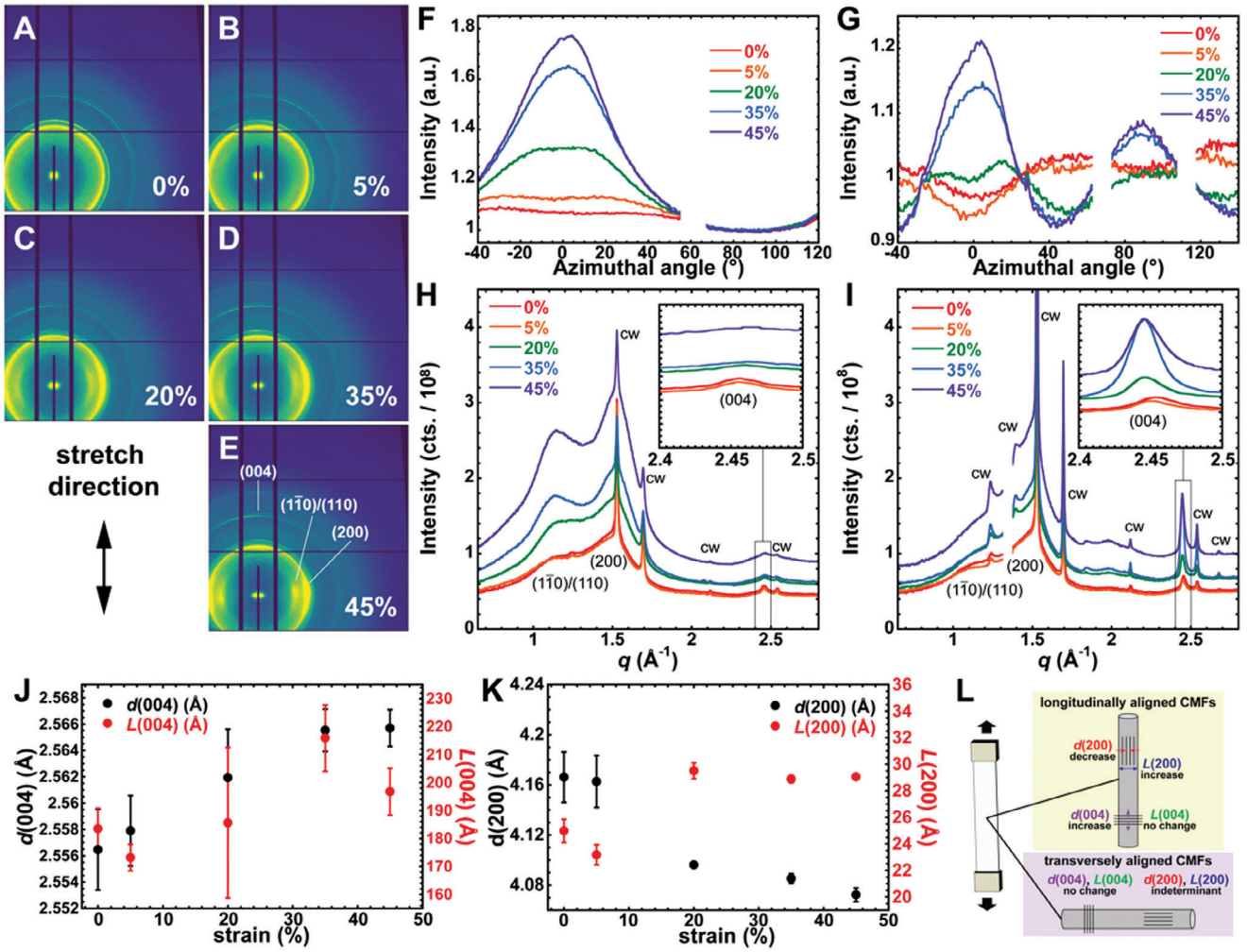

Figure 5. Transmission wide-angle X-ray scattering reveals changes in the dimensions of cellulose chain packing. WAXS 2D images of A) unstretched, B) 5%, C) 20%, D) 35%, and E) 45% strain onion epidermal wall, taken at the Soft Matter Interfaces beamline at National Synchrotron Light Source II, Brookhaven National Laboratory. F,G) Azimuthal intensity profiles integrated at F) 1.00 Å^{-1} < q < 1.25 Å^{-1} and G) 1.45 Å^{-1} < q < 1.50 Å^{-1}, corresponding to (1$\bar{1}$0)/(110) and (200) crystalline cellulose reflections respectively. For comparison, azimuthal intensity profiles were normalized at F) 80° and G) 25° for (1$\bar{1}$0)/(110) and (200) respectively. Sector profiles, integrated at ± 5° along the H) equatorial and I) meridional directions. Diffraction peaks from cuticular wax are labeled (cw). Insets: magnification of (004) reflections. All curves represent an average of three replicates. Missing data points in F, G, and I are due to spacing between detector modules. J) Cellulose (004) lattice spacing d and coherence length L versus strain from meridional sector profile. K) Cellulose (200) lattice spacing d and coherence length L versus strain from equatorial sector profile. Data points represent mean ± SEM for five replicates. L) Cartoon illustration of the effects of longitudinal stretch on (004) and (200) ordering in longitudinally and transversely aligned CMFs.

2.4. Cellulose Crystal Reconfiguration (WAXS)

In addition to the nanoscale measurement from SAXS, we collected transmission WAXS 2D images at SMI, NSLS-II to probe q ranges up to 3.0 Å^{-1} (down to 0.2 nm in real space), which can reveal subtle changes in the dimensions of cellulose chain packing. The 2D WAXS patterns show the alignment of cellulose crystal planes towards the stretch direction at high strain, which is consistent with SAXS and AFM. Sharp peaks at approximately 1.24, 1.53, 1.70, 2.09, 2.12, 2.54, and 2.68 Å^{-1} were attributed to diffraction from cuticular wax.[22] As shown in **Figure 5**A–E, the WAXS patterns appear more isotropic from 0 to 5% strain (Figure 5A–C). At 20%, 35% and 45% strain, the (1$\bar{1}$0)/(110) and (200) reflections become prominent along the equatorial regions (Figure 5D,E), indicating that cellulose crystals are oriented such that CMFs are aligned along the stretching direction.

The azimuthal intensity profiles of the (1$\bar{1}$0)/(110) and (200) reflections quantify the change in cellulose crystal plane angle distributions (Figure 5F,G). This validates the reorientation of cellulose specifically, whereas SAXS may include nanoscale features from matrix components. At 0% and 5% strain, (1$\bar{1}$0)/(110) and (200) are oriented into two uniaxial populations at approximately ± 45° from the longitudinal axis ("bimodal alignment"), seen as peaks at ± 45° (Figure 5F,G). About 5% of microfibrils are aligned bimodally based on the area under the peaks at ± 45° in the 0% and 5% curves. The beam size (200 µm wide × 50 µm tall) was large enough to cover about two cells in the unstretched state. This could be from the bimodal alignment of cellulose crystals in

the thin anticlinal (side) walls[23,24] or a small percentage of microfibrils in the periclinal (flat) walls.[25] Overall, the X-ray intensities as a function of polar angle in unstretched walls are consistent with a cell wall structure that is dominated by multiple lamellae with random cellulose microfibril orientation,[5,10] although the modest enhancement of scattering intensities separated by 90° could indicate a subtle preference for a bimodal cellulose orientation, or a small region of the sample that exhibits a predominant bimodal orientation, similarly to a previous report.[25]

The (200) reflection has peaks at 90° at high strains (Figure 5G), while this is not observed in the azimuthal intensity profiles of $(1\bar{1}0)/(110)$ (Figure 5F). This suggests that cellulose crystal movements are dependent on the orientation of crystal facets with respect to the cell wall plane, previously referred to as crystal texture,[22] such that only cellulose crystals with (200) planes parallel with the cell wall plane can be transverse at high strain. The SAXS azimuthal intensity profiles also do not peak at 90° (Figure 4H), indicating that transverse alignment is not on the size scale of CMF bundles.

Given that the WAXS feature of the unit cell of cellulose Iβ is well established,[26] we can correlate the WAXS reflections to lattice information of CMFs at a specific orientation. The equatorial WAXS profiles contain the information of $(1\bar{1}0)/(110)$ and (200) ordering in longitudinally aligned CMFs and (004) ordering of transversely aligned CMFs (Figure 5H). Conversely, the meridional WAXS profiles contain the information of $(1\bar{1}0)/(110)$ and (200) ordering in transversely aligned CMFs and (004) ordering of longitudinally aligned CMFs (Figure 5I). The overall intensity of the WAXS profiles increases after strain is applied, which could be due to densification of more cell wall material per area, as shown in Figure 1E. The lattice spacing d was calculated from the relationship $d = 2\pi/q$ and the coherence length L from the Scherrer equation ($L = K\lambda/\beta\cos(\theta)$, where K is the dimensionless shape factor 0.9 and β is the FWHM in radians). The (004) region in the equatorial profiles did not change significantly in shape with increasing strain, which shows that a longitudinal stretch had no effect on the crystal structure of transversely aligned microfibrils (Figure 5H). The meridional (004) reflection, however, increases in intensity and appears to shift to lower q with increasing strain (Figure 5I). This resulted in a 0.4% increase in d(004) after 45% strain (Figure 5J), which may be the result of stretching of the cellulose backbone or a reduction in (004) defects. L(004) was not found to change significantly (Figure 5J), indicating that the degree of disorder within cellulose crystallites and the crystal size were not affected.

With increasing strain, d(200) was found to decrease and L(200) was found to increase (Figure 5K). By 45% strain, d(200) decreased by 2.3% ($p < 0.05$, $n = 3$) and L(200) increased by 16.3% ($p < 0.05$, $n = 3$) from the unstretched state. In other words, strain causes tighter (200) chain packing and higher long-range order across crystallites in longitudinally aligned CMFs. Coherence length (L) derived from the Scherrer equation is often described as "crystallite size", but it is highly unlikely that cellulose crystals grow during the mechanical stretch. In polymeric systems, such as cellulose, the coherence length is often dominated by the degree of paracrystalline disorder rather than crystallite size.[27–29] The increase in L(200) more likely corresponds to a reduction in crystal defects or an increase in coherence from aligned cellulose crystals. There was little signal in the (200) region in the meridional profiles at high strains (Figure 5I), indicating small amounts of transverse CMFs. As a result, d(200) and L(200) for the transverse CMFs at high strains were indeterminant. Overall, these results show that under large deformation, cellulose chains oriented in the stretching direction pack more tightly, and their backbones are stretched, indicating that they are effectively bearing substantial loads.

3. Discussion

In this study, we used optical microscopy, AFM, SAXS and WAXS to investigate structures of wall polymers at multiple length scales. While AFM reveals the organization of surface CMF networks at the microscale, transmission X-ray scattering techniques characterize CMF ordering and distribution throughout the cell wall. By comparing wall polymer structures in epidermal cell walls stretched to different degrees, we showed that upon large deformation, the wall undergoes shape changes and CMFs exhibited large-scale rearrangements and nanoscale reconfiguration with various degrees of reversibility. Consistent with previous simulation observations,[8] CMF rearrangements upon tensile stretch are orientation dependent: longitudinally oriented CMFs straighten and align more uniformly while transversely aligned CMFs curve and kink. Kinking of transversely aligned CMFs was observed in previous in situ AFM of hydrated onion cell walls.[10] Both AFM and X-ray data show that CMFs undergo a large degree of realignment before reaching 20% strain, and this realignment continues, albeit to a lesser extent, even at higher strains. Reorientation of transversely curved CMFs may partially contribute to the overall realignment observed in X-ray results. At large strains, a distinct CMF organization emerges: longitudinally aligned CMFs become highly ordered and straight, and they are drawn to ≈7.4 nm center-to-center distance. We propose that 7.4 nm is the closest center-to-center spacing between individual CMFs that are not in a bundle, as illustrated in **Figure 6**. Wall matrix components like pectin or xyloglucan may keep CMFs from moving closer than 7.4 nm upon wall straining. We speculate that the 7.4 nm distance would not be very different in the hydrated state as we have previously reported that pectin spacings along the plane of the cell wall do not collapse after drying in the onion cell wall.[30] Pectin has a persistence length on the scale of 10 nm,[31] so it is likely to have a stiff conformation. Along with CMFs, pectin is also known to reorient towards the stretch direction.[7] The aligned but uncorrelated pectin may act as space fillers that prevent new inter-fibril contacts and irreversible formation of large CMF bundles upon straining, maintaining the cellulose network structure with intertwined yet separated CMFs. Our results show that although wall matrix-like pectins do not directly bear tensile stress due to their small tensile and bending modulus, they may play important roles in preserving the structural integrity of the CMF network during strain.

Several studies of woody cellulose materials have observed the stretching of CMF backbones in the secondary cell wall,[32,33] where CMFs are highly ordered, uniformly aligned, and embedded in lignin and xylan.[34,35] This compact and rigid structure allows CMFs to stretch without extensive sliding. In contrast, CMFs in the primary cell wall are expected to slide before they are subjected to massive stress that may lead to backbone extensions. If we assume that 50% of CMFs reorient towards the stretching

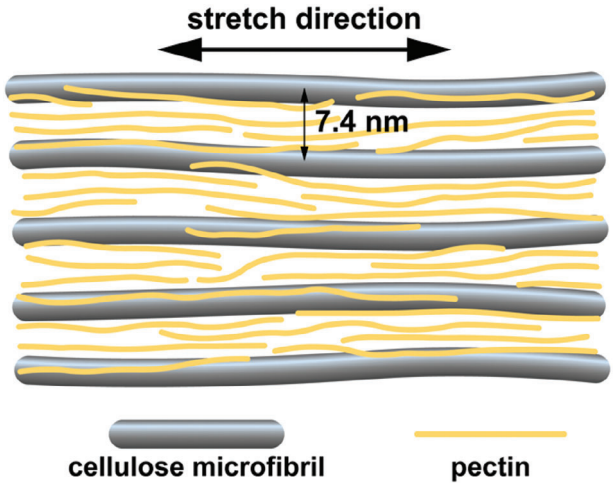

Figure 6. The proposed arrangement of cellulose microfibrils which produces the equatorial diffraction in the SAXS of onion peel at >20% strain. The realignment of CMFs towards the direction of the stretch results in an ordered structure with a center-to-center distance of 7.4 nm. This spacing could be a result of unidirectionally aligned pectin chains filling the spaces between microfibrils.

direction and comprise ≈1.35% of the cross-sectional area of the onion epidermal cell wall,[8] CMFs are expected to bear an average stress of ≈740 MPa in a wall stretched to 45% (total wall stress of ≈10 MPa). In this study, we present experimental evidence showing that for cellulose Iβ oriented towards the stretching direction, the backbone length extended (increase in d(004)) and the chains packed more tightly (decrease in d(200)), indicating that these CMFs bear substantial stress in walls upon extensive deformation. With the Young's modulus of crystalline cellulose Iβ ranging from 107 to 143 GPa,[36,37] stretching the CMF backbone to 0.4% may require stress up to ≈572 MPa, which is roughly comparable to our calculation of the average CMF stress (≈740 MPa) in the 45% strained walls. Thus, a 0.4% local strain of glucan backbones is reasonable for a wall stretched to 45% strain if CMFs bear most of the stress. This indicates that CMF backbones can bear a stress of ≈600 MPa or more without detachment from the cellulose network or failure, showing that CMFs in the primary cell wall are not easily prone to detachment after slippage but can bear substantial stress and resist further slippage during large wall deformations. The 0.4% backbone stretch in this study may be an underestimate as the wall samples were fixed by drying between clamps and were not tensioned during measurements. Some CMFs may have returned to the unstretched form once the wall was removed from the extensometer. In situ characterization of these features in walls under tension will provide more insights into the stress CMFs can bear before failure.

These rearrangements of CMFs at large strains also provide insight into the molecular mechanisms of the linear region in the stress-strain curves of onion epidermal walls. Previous work showed that plastic deformation of cell walls is mainly due to irreversible sliding between CMFs,[8] which may result in extended and thinner CMF bundles. Our results show that even after extensive plastic deformations, CMFs did not bundle into macrofibrils. Instead, thinner CMF bundles may allow further compacting of CMF networks, resulting in increased numbers of longitudinally aligned CMFs spaced 7.4 nm apart at large strains. As a result, they experience compressive forces that increase the yield threshold and require more force to introduce additional sliding. This also enables locally compacted CMFs that are resistant to sliding to undergo further stretching and bear additional stress, as observed in longitudinally aligned CMFs whose backbones further extend as strain increases. Our experimental evidence suggests that the increase in stress, even after the wall starts to yield, may occur from the increased resistance to sliding upon transverse compacting of CMFs. Alternatively, the linear plastic deformation may result from increased numbers of CMFs oriented towards the stretching direction. However, this explanation seems unlikely because similar behavior was observed in cellulose materials that have uniformly aligned CMFs with negligible CMF reorientation.[38] Mechanical analysis of walls with modified dimensional change or wall matrix may be useful to uncover the key factors or components related to increased resistance to plastic deformation.

4. Conclusion

Employing a suite of characterization tools, we show that epidermal cell walls undergo structural changes ranging from mesoscale dimensional alteration to angstrom scale cellulose chain reconfiguration. When stretched by 20%, the wall shrank in the transverse direction where longitudinally aligned CMFs are drawn closer to a more ordered and aligned organization. SAXS revealed a reversible change in anisotropy at strains of 20% or higher, along with the formation of a 7.4 nm spacing along the longitudinal direction. This feature is likely the center-to-center spacing between individual microfibrils, with pectin chains preventing closer contact. WAXS revealed a 0.4% widening of the (004) lattice and a 2.3% decrease of the (200) lattice in longitudinally aligned CMFs at 45% wall strain. Overall, our results showed that upon large deformations, CMFs that are oriented toward the stretching direction become highly ordered and aligned such that CMFs are packed more densely with a 7.4 nm center-to-center distance and that the backbones of glucan chains are increasingly stretched to bear greater loads. These observations shed light on the molecular mechanism of the linear plastic deformation of the wall: the aggregation of longitudinal microfibrils raises the yield threshold for sliding and enables further stretching of the cellulose to bear more load. These results offer insights for the development of biomimetic materials that are both strong and extensible.

5. Experimental Section

Onion Sample Preparation: White onion bulbs (*Allium cepa*) were purchased from local grocery stores. The epidermal walls were isolated by rupturing the cells located at the center of the fifth scale, with the first being the outermost fleshly scale, as previously described.[39] The 7 µm thick epidermal walls were cut into 3 mm wide and 10 mm long strips, washed with 20×10^{-3} M HEPES at pH 7.0 for 5 min, and then rinsed three times with water for 5 min each.

Tensile Tests: The onion strips were stretched to different target strains (0%, 5%, 20%, 35%, 45%, and 50%) using a custom stretching device.[39] Onion strips were clamped at the tissue ends with a 5 mm

clamping distance. The walls were stretched to the target strain at a constant speed of 3 mm min^{-1}. To examine the structural change of the wall upon deformation, the deformed wall samples were fixed by air drying them while under tension for 30 min (stretch and dry under tension), then carefully removed them from the clamp. To observe only the irreversible part of the structural change, the wall stretched to 45% was released from tension and dried in air without any applied stress (stretch and relax).

Peel Deformation Imaging: A customized stage consisting of a linear actuator (New Scale Technologies M3-LS) and a load cell (Futek LSB200) was positioned under a microscope with a camera. New Scale software was used to control the actuator and monitor the position. QuickDAQ software was used to acquire the load cell signal and monitor the applied load. The clamp distance of this device was 5 mm, the same as the distance used in mechanical tests. For imaging purposes, onion strips were put on a glass slide so peels could stay in the focal plane during deformation. A trimmed cover slip (3 mm × 10 mm) was placed across the peel to minimize the formation of wrinkles during stretching, allowing a more accurate measurement of cell deformations. The stretching speed was set to 50.5 µm s^{-1} (strain rate of 0.01 s^{-1}) with a target strain of 50% (2500 µm extension). For time-lapse imaging, the time interval for each frame was 1 s. Stretching and time-lapse imaging were started simultaneously, allowing us to capture an image every time the wall was stretched by 1%. To calculate Poisson's ratio, the longitudinal and transverse aspects of cells were measured when the wall was stretched to different strains. At each strain, the longitudinal and transverse strain was calculated relative to the original cell aspects at 0%. To estimate the cell wall area at different strain levels, the epidermal wall area of each cell (as outlined by anticlinal walls) was delineated and measured. ImageJ was used for all the measurements.

Atomic Force Microscopy Imaging: To remove the surface debris for AFM imaging, the epidermal walls were washed in 2% sodium dodecyl sulfate (SDS) for 30 min and then rinsed three times with water for 5 min each. The onion epidermal walls were then stretched to different strains (0%, 5%, 20%, 35%, and 50%). To remove the surface pectin layer and reveal the cellulose structures after dehydration, the cell walls were treated with 10 µg mL^{-1} pectate lyase (PL) in 50 × 10^{-3} M N-cyclohexyl-3-aminopropanesulfonic acid (CAPS), pH 10 buffer with 2 × 10^{-3} M Ca^{2+} for 15 min while they were under strain. The recombinant PL (from *Cellvibrio japonicas*; E-PLYCJ) was purchased from Megazyme. Following the 15 min PL treatment, the wall was thoroughly washed with water five times. Finally, the wall was air-dried for 30 min under tension (except for unstretched and relaxed walls) and carefully removed from the stretching stage for AFM imaging. Three sets of walls stretched to a series of target strains with each set from a different onion were prepared. The stretched and dried walls were fixed onto glass slides with nail polish with the wall surface facing upwards for scanning in air. AFM topography images were collected with a Dimension Icon AFM (Bruker, CA, USA), operated in PeakForce tapping mode with ScanAsyst and Quantitative Nanomechanical Mapping. A ScanAsyst Air probe was used, which has a spring constant of ≈0.4 N m^{-1} and a sharp silicon tip with ≈2 nm radius, 5 µm height, 15° front angle, 25° back angle, and 17.5° side angle. For each epidermal wall sample, we selected at least three cells and captured 2 µm × 2 µm images at a resolution of 512 × 512 pixels with a setpoint of ≈1 nN and scanning rate of ≈0.8 Hz. All the height images were plane fit to fourth order and flattened to second order to remove surface slope and tilt. The images were exported in TIFF format by Nanoscope Analysis. An ImageJ plugin OrientationJ[40] was used to measure the orientation distribution of surface cellulose microfibrils.

Small/Wide-Angle X-Ray Scattering Measurements and Analysis: After drying, onion peels were adhered to washers using epoxy and mounted into the X-ray scattering sample chamber with the longitudinal cell direction in the vertical direction. Each onion peel sample was measured at 2–4 spots along the horizontal center of the peel, with the averaged data of the spots representing one replicate.

Onion peels that were stretched and dried under tension were measured at the Soft Matter Interfaces (SMI) beamline (12-ID) at the National Synchrotron Light Source II at Brookhaven National Laboratory. Samples were measured with a 16.1 keV X-ray beam 200 µm wide × 50 µm tall in a vacuum (5 × 10^{-3} torr) environment. SAXS was collected with a Pilatus 1 M detector at a distance 5 m away from the sample. WAXS was collected with a Pilatus 900KW detector at a distance 280 mm away from the sample, rotating at a fixed arc along the 2θ direction to cover a wider q-range. Detector image stitching and data reduction from 2D images to 1D plots was performed using the SMI analysis package on Jupyter Notebook.

Onion peels which were stretched and relaxed were measured at beamline 7.3.3 at the Advanced Light Source (ALS) at Lawrence Berkeley National Laboratory. Samples were measured with a 10 keV X-ray beam 300 µm wide × 70 µm tall. SAXS measurements were conducted in air at a distance 3.5 m from the sample. Air scattering was mitigated by minimizing the distance between the X-ray tube and the sample. SAXS was collected with a Pilatus 2 M detector. Data reduction from 2D images to 1D plots was performed using Nika on Igor Pro.[41]

For each setup, scattering was collected with no sample in the beam path and subtracted as the instrumental background. For scattering collected on Pilatus 1 M and 2 M detectors, scattering was collected at two different detector heights and the two images were stitched together to fill in the regions of empty data between detector modules. Sector profiles for SAXS and WAXS were obtained by azimuthally integrating the images ± 5° from the horizontal direction (equatorial) or from the vertical direction (meridional). The (200) region of the equatorial WAXS profiles were fitted using previously described methods.[30] The (200) region of the meridional WAXS profiles of samples at high strain were unable to be fit for quantitative analysis due to low cellulose signal and dominance of diffraction from cuticular wax. The (004) region of the meridional WAXS profiles was fitted to a Gaussian distribution with a linear background to extract d(004) and L(004). Azimuthal intensity profiles were obtained by integrating the images from 0.01 $Å^{-1} < q < 0.1$ $Å^{-1}$ for SAXS, 1.00 $Å^{-1} < q < 1.25$ $Å^{-1}$ for the $(1\bar{1}0)/(110)$ crystalline cellulose reflection in WAXS, and 1.45 $Å^{-1} < q < 1.50$ $Å^{-1}$ for the (200) crystalline cellulose reflection in WAXS. The FWHM of the SAXS azimuthal intensity profiles were obtained by fitting the profiles with a Lorentzian distribution with a flat linear background. Tests for statistical significance for FWHM, d, and L are two-tailed Student's t-tests with n number of replicates (onions), where two groups are considered significantly different if probability $p < 0.05$.

Supporting Information

Supporting Information is available from the Wiley Online Library or from the author.

Acknowledgements

J.Y. and J.T.D. contributed equally to this work. This work was supported as part of the Center for Lignocellulose Structure and Formation, an Energy Frontier Research Center funded by the U.S. Department of Energy, Office of Science, Basic Energy Sciences under award DE-SC0001090. The National Synchrotron Radiation Light Source II at Brookhaven National Laboratory is supported by the Office of Science and Office of Basic Energy Sciences, of the U.S. Department of Energy under Contract No. DE-SC0012704. The Advanced Light Source at Lawrence Berkeley National Laboratory is supported by the Director, Office of Science, Office of Basic Energy Sciences, of the U.S. Department of Energy under Contract No. DE-AC02-05CH11231. Partial support for J.Y. for microscopic image analysis came from the Center for Engineering MechanoBiology, an NSF Science and Technology Center, under Grant agreement No. CMMI: 15-48571. The authors thank Liza Wilson and Chenhui Zhu for their technical assistance.

Conflict of Interest

The authors declare no conflict of interest.

Data Availability Statement

The data that support the findings of this study are available from the corresponding author upon reasonable request.

Keywords

atomic force microscopy, plant epidermal cell walls, small-angle X-ray scattering, strain-hardening, wide-angle X-ray scattering

Received: December 18, 2023
Revised: February 5, 2024
Published online: February 22, 2024

[1] D. J. Cosgrove, *Plant Physiol.* **2022**, *189*, 1246.
[2] E. Coen, D. J. Cosgrove, *Science* **2023**, *379*, eade8055.
[3] T. Zhang, S. Mahgsoudy-Louyeh, B. Tittmann, D. J. Cosgrove, *Cellulose* **2014**, *21*, 853.
[4] T. Zhang, H. Tang, D. Vavylonis, D. J. Cosgrove, *Plant J.* **2019**, *100*, 1101.
[5] T. Zhang, Y. Zheng, D. J. Cosgrove, *Plant J.* **2016**, *85*, 179.
[6] M. S. Zamil, H. Yi, M. A. Haque, V. M. Puri, *Am. J. Bot.* **2013**, *100*, 1105.
[7] K. Kafle, Y. B. Park, C. M. Lee, J. J. Stapleton, S. N. Kiemle, D. J. Cosgrove, S. H. Kim, *Cellulose* **2017**, *24*, 3145.
[8] Y. Zhang, J. Yu, X. Wang, D. M. Durachko, S. Zhang, D. J. Cosgrove, *Science* **2021**, *372*, 706.
[9] J. Yu, Y. Zhang, D. J. Cosgrove, *Proc. Natl. Acad. Sci. USA* **2024**, *121*, 2316396121.
[10] T. Zhang, D. Vavylonis, D. M. Durachko, D. J. Cosgrove, *Nat Plants* **2017**, *3*, 17056.
[11] R. H. Wilson, A. C. Smith, M. Kacurakova, P. K. Saunders, N. Wellner, K. W. Waldron, *Plant Physiol.* **2000**, *124*, 397.
[12] D. Chen, L. D. Melton, D. J. Mcgillivray, T. M. Ryan, P. J. Harris, *Planta* **2019**, *250*, 1819.
[13] F. Saxe, M. Eder, G. Benecke, B. Aichmayer, P. Fratzl, I. Burgert, M. Rüggeberg, *Plant Methods* **2014**, *10*, 25.
[14] M. Rüggeberg, F. Saxe, T. H. Metzger, B. Sundberg, P. Fratzl, I. Burgert, *J. Struct. Biol.* **2013**, *183*, 419.
[15] W. Gindl, K. J. Martinschitz, P. Boesecke, J. Keckes, *Compos. Sci. Technol.* **2006**, *66*, 2639.
[16] S. Huang, M. Makarem, S. N. Kiemle, Y. Zheng, X. He, D. Ye, E. W. Gomez, E. D. Gomez, D. J. Cosgrove, S. H. Kim, *Carbohydr. Polym.* **2018**, *197*, 337.
[17] L. M. Chen, R. H. Wilson, M. C. McCann, *J. Mol. Struct.* **1997**, *408*, 257.
[18] K. Kafle, X. Xi, C. M. Lee, B. R. Tittmann, D. J. Cosgrove, Y. B. Park, S. H. Kim, *Cellulose* **2014**, *21*, 1075.
[19] J. Fahlén, The cell wall ultrastructure of wood fibres : effects of the chemical pulp fibre line, https://www.semanticscholar.org/paper/The-cell-wall-ultrastructure-of-wood-fibres-%3A-of-Fahl%C3%A9n/5e9bab1e4c590f2492a3aac783e6457ff1045709 (accessed: February 2024).
[20] K. Koljonen, M. Österberg, M. Kleen, A. Fuhrmann, P. Stenius, *Cellulose* **2004**, *11*, 209.
[21] A. Hexemer, W. Bras, J. Glossinger, E. Schaible, E. Gann, R. Kirian, A. MacDowell, M. Church, B. Rude, H. Padmore, *J. Phys.: Conf. Ser.* **2010**, *247*, 012007.
[22] D. Ye, S. Rongpipi, S. N. Kiemle, W. J. Barnes, A. M. Chaves, C. Zhu, V. A. Norman, A. Liebman-Peláez, A. Hexemer, M. F. Toney, A. W. Roberts, C. T. Anderson, D. J. Cosgrove, E. W. Gomez, E. D. Gomez, *Nat. Commun.* **2020**, *11*, 4720.
[23] X. Xi, S. H. Kim, B. Tittmann, *J. Appl. Phys.* **2015**, *117*, 024703.
[24] J. Lee, J. Choi, L. Feng, J. Yu, Y. Zheng, Q. Zhang, Y.-T. Lin, S. Sah, Y. Gu, S. Zhang, D. J. Cosgrove, S. H. Kim, *Biomacromolecules* **2023**, *24*, 4759.
[25] W. J. Nicolas, F. Fassler, P. Dutka, F. K. M. Schur, G. Jensen, E. Meyerowitz, *Curr. Biol.* **2022**, *32*, 2375.
[26] Y. Nishiyama, P. Langan, H. Chanzy, *J. Am. Chem. Soc.* **2002**, *124*, 9074.
[27] J. Rivnay, R. Noriega, R. J. Kline, A. Salleo, M. F. Toney, *Phys. Rev. B* **2011**, *84*, 045203.
[28] D. M. DeLongchamp, R. J. Kline, in *Organic Electronics II: More Materials and Applications* (Ed.: H. Klauk) Wiley, New York **2012**, pp. 27–101.
[29] W. Zhang, J. H. Bombile, A. R. Weisen, R. Xie, R. H. Colby, M. J. Janik, S. T. Milner, E. D. Gomez, *Macromol. Rapid Commun.* **2019**, *40*, 1900134.
[30] J. T. Del Mundo, S. Rongpipi, H. Yang, D. Ye, S. N. Kiemle, S. L. Moffitt, C. L. Troxel, M. F. Toney, C. Zhu, J. D. Kubicki, D. J. Cosgrove, E. W. Gomez, E. D. Gomez, *Sci. Rep.* **2023**, *13*, 5421.
[31] A. Zdunek, P. M. Pieczywek, J. Cybulska, *Compr. Rev. Food Sci. Food Saf.* **2021**, *20*, 1101.
[32] L. H. Thomas, C. M. Altaner, V. T. Forsyth, E. Mossou, C. J. Kennedy, A. Martel, M. C. Jarvis, *Sci. Rep.* **2021**, *11*, 453.
[33] N. Gierlinger, *Appl. Spectrosc. Rev.* **2018**, *53*, 517.
[34] O. M. Terrett, J. J. Lyczakowski, L. Yu, D. Iuga, W. T. Franks, S. P. Brown, R. Dupree, P. Dupree, *Nat. Commun.* **2019**, *10*, 4978.
[35] D. J. Cosgrove, M. C. Jarvis, *Front. Plant Sci.* **2012**, *3*, 204.
[36] A. Šturcová, G. R. Davies, S. J. Eichhorn, *Biomacromolecules* **2005**, *6*, 1055.
[37] X. Wu, R. J. Moon, A. Martini, *Cellulose* **2014**, *21*, 2233.
[38] N. Mittal, F. Ansari, V. K. Gowda, C. Brouzet, P. Chen, P. T. Larsson, S. V. Roth, F. Lundell, L. Wågberg, N. A. Kotov, L. D. Söderberg, *ACS Nano* **2018**, *12*, 6378.
[39] D. Durachko, Y. B. Park, T. Zhang, D. Cosgrove, *Bio- Protoc* **2017**, *7*, 2662.
[40] Z. Püspöki, M. Storath, D. Sage, M. Unser, in *Focus on Bio-Image Informatics*, Springer International Publishing, New York **2016**, pp. 69–93.
[41] J. Ilavsky, *J. Appl. Crystallogr.* **2012**, *45*, 324.